Research Article Vol. 65, No. 5 / 10 February 2026 / Applied Optics 1511

applied optics

Broadband birefringence phase-matched second-harmonic generation in a slightly curved lithium niobate-on-insulator waveguide

Xingze Song,[1] Yongzhi Tang,[1] Tingting Ding,[2] Wenjun Ding,[1] Jing Qiu,[1,3] Zengya Li,[1] Jianbiao Dai,[1] Hao Li,[1] Shijie Liu,[1] Xianfeng Chen,[1,3,4,5] Jing Zhang,[6,7] and Yuanlin Zheng[1,3,4,8]

[1]State Key Laboratory of Advanced Optical Communication Systems and Networks, School of Physics and Astronomy, Shanghai Jiao Tong University, Shanghai 200240, China
[2]School of Electronic and Electrical Engineering, Shanghai University of Engineering Science, Shanghai 201620, China
[3]Zhangjiang Laboratory, Shanghai 201210, China
[4]Shanghai Research Center for Quantum Sciences, Shanghai 201315, China
[5]Collaborative Innovation Center of Light Manipulations and Applications, Shandong Normal University, Jinan 250358, China
[6]Institute of Semiconductors, Chinese Academy of Sciences, Beijing 100083, China
[7]jingsz@semi.ac.cn
[8]ylzheng@sjtu.edu.cn

Received 3 December 2025; accepted 5 January 2026; posted 7 January 2026; published 3 February 2026

Lithium niobate-on-insulator (LNOI) waveguides, leveraging their excellent optical field confinement and high nonlinear coefficients, have become an ideal platform for achieving optical frequency conversion. Phase-matching interaction strength and bandwidth are critical factors in this process. Here, we propose a scheme using micrometer-scale, slightly curved waveguides on x-cut LNOI to achieve broadband birefringence phase matching (BPM). Experimentally, we observed a broadband second-harmonic generation (SHG) with a bandwidth exceeding 100 nm in the near-infrared regime, achieving the highest, to the best of our knowledge, normalized conversion efficiency of 1.38%/(W · cm^2) at 1560 nm. For 500 fs pulsed light pumping, an absolute conversion efficiency of over 10% is achieved at a low input power. The approach is suitable for frequency conversion of ultrashort lasers on a chip. This approach presents a promising alternative to periodically poled lithium niobate (PPLN) for broadband frequency conversion applications.

https://doi.org/10.1364/AO.586578

1. INTRODUCTION

Second-order nonlinear wave mixings, for example, second-harmonic generation (SHG), are essential optical processes for applications in wavelength conversion [1–3], infrared photon generation [4], detection [5], and photon pair sources [6,7]. In areas such as optical information communication, ultrafast pulsed lasers, and spectroscopy, broadband frequency conversion is crucial for enabling technologies such as all-optical signal processing [8,9], optical frequency combs [10,11], and supercontinuum generation [12–14].

Lithium niobate-on-insulator (LNOI) has emerged as an ideal platform for such processes [15–17], especially when implemented in micro- and sub-micrometer scales [18–20]. Efficient second-order nonlinear processes rely on robust phase-matching interactions. The significant refractive index contrast between the waveguide and its surroundings strongly confines the optical field within the waveguide, substantially enhancing nonlinear efficiency and allowing for flexible control over mode field and effective refractive index. Leveraging LN's ferroelectric properties and optical anisotropy, various phase-matching schemes, including birefringent phase matching (BPM), quasi-phase matching (QPM), and modal phase matching (MPM), have been implemented in LNOI waveguides. For QPM, by optimizing the domain structure in periodically poled lithium niobate (PPLN), the SHG conversion efficiency in thin-film lithium niobate (TFLN) nanowaveguides has reached over 2000%/(W · cm^2) [21–23]. Although BPM or MPM offers lower conversion efficiency, it provides advantages such as ease of temperature tuning, and the avoidance of poling processes [24,25].

There is a significant trade-off for the phase-matching bandwidth due to material dispersion and long interaction length. Phase-matching bandwidths are generally limited to much narrower than 10 nm for 1 cm long LN waveguides, making

it challenging to meet the needs of broadband frequency conversion devices. Previous effects involve temperature gradient along the waveguide [24], dispersion engineering [26–28], chirped PPLN [13,29,30], mode hybridization [31], or coupled waveguides [32,33], which have quite high requirements for technological processes. Dispersion engineering is the most widely used method to enhance phase-matching bandwidth, often achieved by tailoring the waveguide's geometric structure, including cross-sectional shape and etching depth [34,35]. Dispersion engineering can be combined with various phase-matching techniques to enhance phase-matching bandwidth without compromising interaction length. At submicrometer scales, the mode refractive index becomes sensitive to waveguide structure changes, which also affects mode transmittance, potentially impacting nonlinear conversion efficiency. Another common approach involves sacrificing the interaction length to enhance the bandwidth. A step-chirped design achieves quasi-phase matching at different wavelengths by implementing a stepped periodic poling structure along the same waveguide [30,36]. The chirped poled TFLN nanowaveguide can achieve octave-spanning SHG with high efficiency. However, precise control of the poling duty cycle remains challenging and is a key factor affecting conversion efficiency.

Here, we present a simplified scheme for broadband frequency conversion based on Type-I BPM SHG on an x-cut LNOI chip using a slightly curved ridge waveguide configuration. SHG is achieved in the whole 1510–1610 nm range with an SHG conversion efficiency of up to 1.38%/(W · cm^2). In the 1530–1560 nm range, SHG is generated using a femtosecond laser with 10.8% on-chip conversion efficiency at low input power.

The cross-section of the x-cut LNOI waveguide is shown in Fig. 1. The LNOI waveguide has a height of 3 μm, an etch depth of 2 μm, and an etching angle of 60°. The upper width varies from 3 to 6 μm (4.5 μm in Fig. 1). A 0.3 μm thick silica coating layer covers the sample for protection. The waveguide cross-section lies in the xz plane. The BPM angle (θ) is the angle between the wave propagation direction and the optic axis, as shown in the inset of Fig. 1. The waveguide is slightly curved, with a curvature radius (R) of 45 cm, and has a total length of 1.8 cm. Correspondingly, the BPM angle gradually varies from 60° to 62.3°. For Type-I phase matching, FW and SH light exist in the forms of o light (TM mode) and e light (TE mode), respectively. The phase-matching condition is expressed as $n_o(\omega) = n_e(2\omega, \theta)$, where $n_e(2\omega, \theta)$ is defined by $\frac{1}{n_e^2(2\omega,\theta)} = \frac{\cos^2\theta}{n_o^2(2\omega)} + \frac{\sin^2\theta}{n_e^2(2\omega)}$, with θ being the angle between the wave propagation direction and the optic axis. Effective refractive indices in the waveguide are then obtained through numerical simulations using a mode solver. The simulated fundamental transverse modes of FW and SH in the micro-waveguide is given in Fig. 2(a), which shows similar profiles indicating good mode overlap. Since the waveguide is only slightly bent, the fundamental transverse modes can be maintained in the multi-mode waveguide without mode hybridization. Following the parameters given, Fig. 2(b) shows the feasibility that $n_o(\omega)$ lies between $n_o(2\omega)$ and $n_e(2\omega)$. Phase-matching angles of different wavelengths are shown in Fig. 2(c). When the pump light propagates in the curved

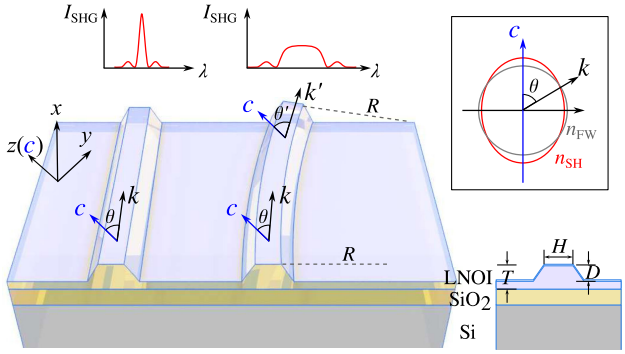

Fig. 1. Schematic of SHG in the straight and curved LNOI waveguides. The waveguide has a curvature radius $R = 45$ cm with a bend angle of 2.3° in a total length of 1.8 cm. Inset: BPM scheme.

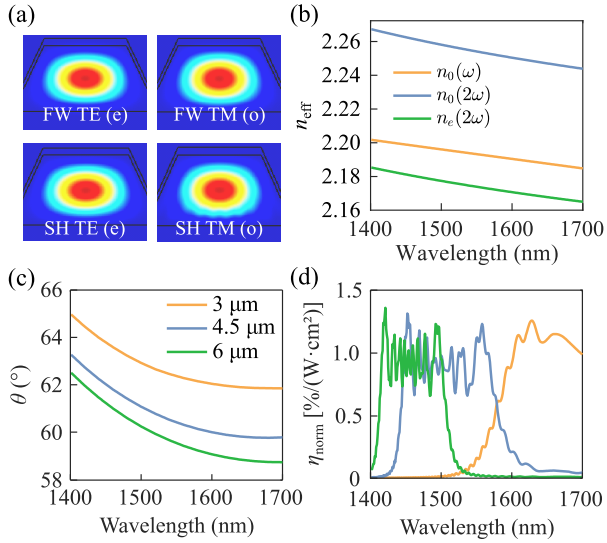

Fig. 2. (a) TE and TM fundamental modes of 1550 nm FW and 775 nm SH waves, respectively. (b) Effective refractive indices of FW and SH light varying with FW wavelength. (c) Theoretical BPM angle with respect to the FW wavelength for different waveguide top width. (d) Simulated BPM spectra for different waveguide top width as the BPM angle is linearly varying along the propagation direction.

waveguide, the phase-matching condition is met at different wavelengths as the BPM angle varies.

The theoretical BPM spectrum is calculated using the coupled wave equation under the small signal approximation. The propagation of light in a nonlinear waveguide is governed by

$$\frac{dA_2}{dz'} = \frac{i\omega_2^2 d_{eff}}{k_2 c^2} A_1^2 \cdot \exp[-i\Delta\varphi(z')], \quad (1)$$

where k_2 and ω_2 are the wave vector and the angular frequency of SH light. c is the speed of light in vacuum, and z' is the propagation distance. d_{eff} corresponding to the nonlinear coefficient d_{31} is 4.6 pm/V. A_1 and A_2 are complex amplitudes for FW and SH, respectively. $\Delta\varphi(z') = \int_0^z \Delta k(z') \cdot dz'$ reflects phase mismatch (Δk) induced phase difference. In the case of propagation in a curved birefringent waveguide, $\Delta k(z')$ is varying due to the change of angle between the propagating direction and the optic

axis. SH waves of different wavelengths are generated from different regions, which is similar to that in chirped or step-chirped QPM schemes [3,30]. Figure 2(d) shows the simulation results of bandwidth and normalized efficiency of SH light under the above conditions.

2. RESULTS

In our experiment, the waveguides are fabricated from a commercial x-cut micrometer thick LNOI wafer (NANOLN). The 3 μm thick LN layer on top of a 2 μm silica buffering layer on a silicon substrate is formed from direct mechanical thinning and chemo-mechanical polishing procedures. The waveguide is then fabricated using UV lithography and deep dry etching. The fabrication details are similar to those in Ref. [1]. The direction of the waveguide with respect to the optic axis is well defined during UV lithography with an accuracy of 0.2°. Both ends of the LNOI waveguide are finely polished, but without anti-reflection coating, for light coupling. The top widths of the fabricated waveguide samples are 3.0, 4.5, and 6.0 μm. The sidewall angle is approximately 60°. The length of the waveguides is 1.5 cm. Figures 3(a) and 3(b) show the optical microscopy images of the front and rear ends of the waveguide, respectively, showing that the waveguide is only slightly bent.

Figure 3(c) provides a schematic of the SHG experimental setup, where the continuous wave (cw) pump light (Toptica CTL, 1510–1630 nm) passes through a polarization controller (PC) before being coupled in and out of the waveguide via a pair of lensed optical fibers. The transmitted light is filtered by a wavelength division multiplexer (WDM), allowing the observation of the spectrum with a power meter. Figure 3(d) shows the transmission of 1550 nm light in waveguides with different top widths. For the 3 μm width, the small waveguide size amplifies the transmission loss caused by waveguide bending, significantly affecting the frequency conversion. Figures 3(e)–3(g) present the second harmonic spectra of waveguides with different widths. The conversion band shifts toward shorter wavelengths as the width increases, consistent with the simulation results in Fig. 2(d). Given the frequency range limitations of the continuous wave laser, only the conversion band of the 4.5 μm width waveguide was fully measurable, showing a bandwidth and range closely aligned with simulation results.

For the 4.5 and 6 μm LNOI waveguides, which exhibit relatively high coupling efficiency, the normalized second harmonic conversion efficiency is defined as $\eta_{\text{norm}} = P_2(L)/P_1^2(0)L^2$, where P_2 and P_1 are SH and FW power, respectively, and L is the waveguide length. Figure 4 shows the experimental measurement results of the normalized conversion efficiency compared with theoretical calculations. In the 3 μm width waveguide, the highest conversion efficiency occurs at the fundamental wavelength of 1560 nm, with a value of $0.42\%/(\text{W}\cdot\text{cm}^2)$, as shown in Fig. 4(a). In the 4.5 μm width waveguide, the highest conversion efficiency occurs at the fundamental wavelength of 1560 nm, reaching a value of $1.38\%/(\text{W}\cdot\text{cm}^2)$, as shown in Fig. 4(b). Additionally, under the conditions of constant bending radius and initial angle with a waveguide width of 4.5 μm, the bending angles were adjusted to 1.8° and 1.3°, respectively, for waveguide fabrication and experimental testing. The bent section of the waveguide was connected to a straight waveguide,

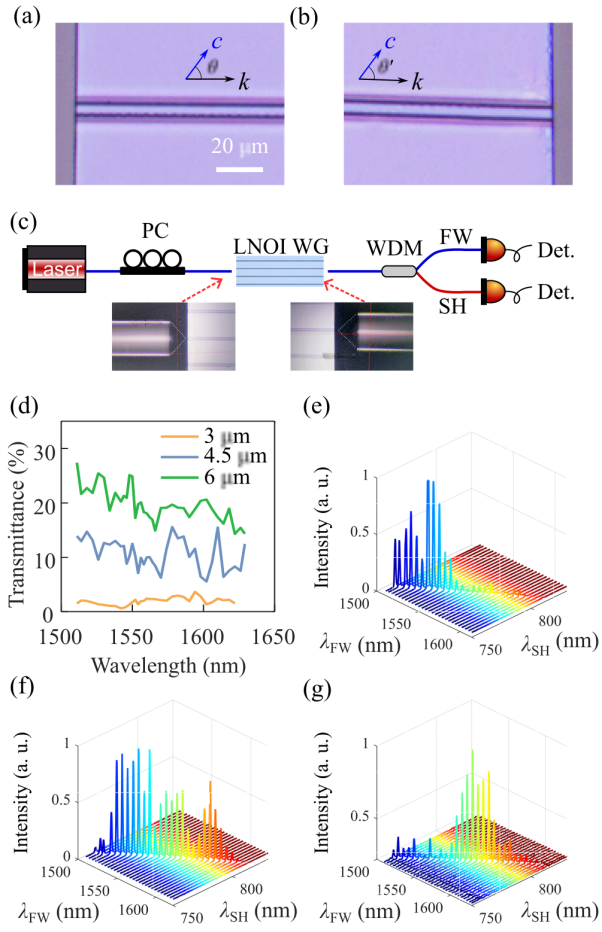

Fig. 3. Microscopy top view of the: (a) front and (b) rear ends of the waveguide. (c) Schematic of the SHG experimental setup. PC, polarization controller; LNOI WG, LNOI waveguide; WDM, wavelength division multiplexing; FW: fundamental wave; SH, second harmonic; and Det., detector. (d) Measurement of the light coupling efficiency. SH spectra of the (e) 6, (f) 4.5, and (g) 3 micron width waveguides as the cw pump sweeps from 1510 to 1630 nm.

ensuring the total waveguide length remained unchanged. The comparison between theoretical and experimental results indicates that the normalized conversion efficiency achievable in the experiment approaches the theoretical value. The measured bandwidth also aligns well with the calculated results. The discrepancies of the bandwidth range may stem from the simulation conditions of the straight waveguide and mode hybridization caused by the relatively large waveguide width. The results also indicate that reducing the angle did not lead to a significant decrease in bandwidth, as the phase-matching angle range predominantly falls within the flat region depicted in Fig. 2(c). The highest peaks in the spectra in Figs. 4(c) and 4(d) originate from the straight part of the waveguide, fully validating the correctness of the theoretical model and the feasibility of the proposed approach. Nonetheless, the 4.5 μm width waveguide achieved broadband frequency conversion with a bandwidth of over 100 nm around the 1550 nm band, meeting our expectations. Compared to the chirped polarization scheme, the normalized efficiency of this scheme is lower by

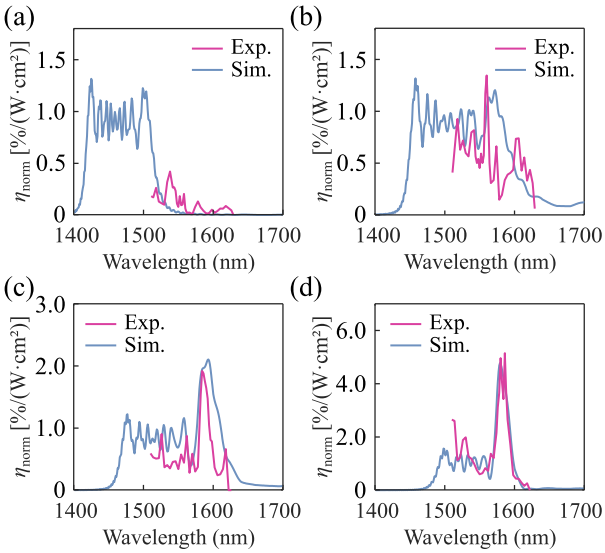

Fig. 4. Simulated and experimental results for (a) the 6 μm width waveguide with a bending angle of 2.3°, (b) the 4.5 μm width waveguide with a bending angle of 2.3°, (c) the 4.5 μm-width waveguide with a bending angle of 1.8°, and (d) the 4.5 μm width waveguide with a bending angle of 1.3°.

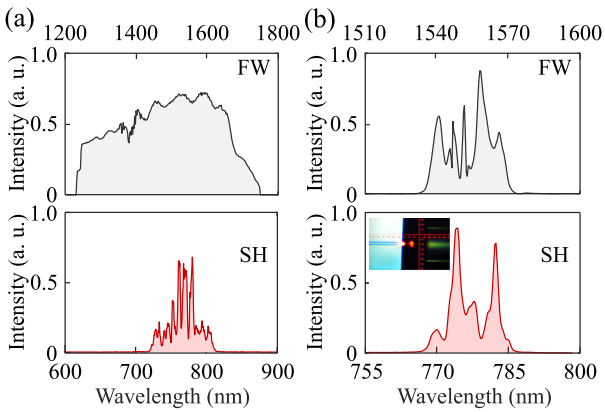

Fig. 5. Demonstration of broadband BPM using wide-bandwidth sources. (a) Spectra of supercontinuum (FW) and its SH. (b) Spectra of fs laser (FW) and its SH.

an order of magnitude, primarily due to the difference between the nonlinear coefficients d_{31} and d_{33}.

To further assess the performance of the waveguide, a supercontinuum laser was used to pump the 4.5 μm width waveguide, and the complete second harmonic bandwidth was measured with a spectrometer. The result shows a 3 dB bandwidth exceeding 100 nm, as shown in Fig. 5(a). The SH signal at the edges of the frequency band provides some evidence for the presence of mode hybridization. The supercontinuum SHG experimental results indicate that the SHG conversion bandwidth of the waveguide meets the requirements, while the conversion efficiency-wavelength curve could be further improved due to mode hybridization caused by the wide-width curved waveguide. Specifically, reducing the mode loss of the waveguide can not only enhance conversion efficiency but also make it possible to further reduce the waveguide width, thereby enhancing the localization of the optical field. The improvement in waveguide transmittance can be achieved by reducing the curvature angle, improving the etching process, or performing mode control under curved waveguide conditions. To simulate practical application conditions, we used a femtosecond fiber laser (500 fs duration, 80 MHz repetition rate) for pumping. Figure 5(b) shows the spectra of fs laser and its SH. The power of the fundamental light passing through the waveguide was 0.749 mW, resulting in an SHG power of 80.7 μW, with an on-chip conversion efficiency of 10.8%. The red light spot that appears at the end of the waveguide and the fiber head can be clearly observed at the coupling point of the output end.

3. CONCLUSION

In conclusion, we demonstrate a broadband BPM SHG in the telecom band with a bandwidth exceeding 100 nm in a micrometer-scale, slightly curved LNOI waveguide. The highest normalized conversion efficiency of 1.38%/(W · cm^2) is obtained at 1560 nm. Under 500 fs pulse light pumping, an absolute conversion efficiency of 10.8% is achieved. This scheme provides a new method for broadband nonlinear frequency conversion, which eliminates the need for poling, offers potentially sensitive temperature tenability [24,25], and can, in principle, be applied to a wider wavelength range through adjustments of the waveguide dimensions and angles. Overall, this study holds significant research and application value for broadband frequency conversion in both continuous and pulsed light sources.

Funding. National Key Research and Development Program of China (2022YFA1205100, 2023YFA1407200); National Natural Science Foundation of China (12192252, 12074252, 62105323, 12504390); Science and Technology Commission of Shanghai Municipality (24JD1401700); Shanghai Municipal Science and Technology Major Project (2019SHZDZX01-ZX06); Innovation Program for Quantum Science and Technology (2021ZD0300802); Yangyang Development Fund.

Disclosures. The authors declare no conflicts of interest.

Data availability. Data underlying the results presented in this paper are not publicly available at this time but may be obtained from the authors upon reasonable request.

REFERENCES

1. Y. Zhang, H. Li, T. Ding, *et al.*, "Scalable, fiber-compatible lithium-niobate-on-insulator micro-waveguides for efficient nonlinear photonics," Optica **10**, 688–692 (2023).
2. X. Wu, Z. Hao, F. Bo, *et al.*, "Advances in second-order nonlinear optical effects of lithium niobate micro/nano waveguides," Chin. Sci. Bull. **67**, 3915–3927 (2022).
3. J. Lin, Y. Xu, J. Ni, *et al.*, "Phase-matched second-harmonic generation in an on-chip $LiNbO_3$ microresonator," Phys. Rev. Appl. **6**, 014002 (2016).
4. N. A. Harper, E. Y. Hwang, R. Sekine, *et al.*, "Highly efficient visible and near-IR photon pair generation with thin-film lithium niobate," Opt. Quantum **2**, 103–109 (2024).
5. S. Dello Russo, A. Elefante, D. Dequal, *et al.*, "Advances in mid-infrared single-photon detection," Photonics **9**, 470 (2022).
6. P. Kumar, S. Saravi, T. Pertsch, *et al.*, "Polarization-entangled photon-pair generation in thin-film lithium niobate waveguides," in *Quantum 2.0 Conference and Exhibition* (Optica Publishing Group, 2024), paper QW3A.43.

7. J. Zhao, C. Ma, M. Rüsing, *et al.*, "High quality entangled photon pair generation in periodically poled thin-film lithium niobate waveguides," Phys. Rev. Lett. **124**, 163603 (2020).
8. J. Wei, C. Cheng, Y. Wu, *et al.*, "Efficient and broadband all-optical wavelength conversion between C and O bands in nanophotonic lithium niobate waveguides," J. Lightwave Technol. **42**, 5966–5973 (2024).
9. C. Lu, B. Zhu, C. Zhu, *et al.*, "All-optical logic gates and a half-adder based on lithium niobate photonic crystal micro-cavities," Chin. Opt. Lett. **17**, 072301 (2019).
10. K. Zhang, W. Sun, Y. Chen, *et al.*, "A power-efficient integrated lithium niobate electro-optic comb generator," Commun. Phys. **6**, 17 (2023).
11. M. Zhang, B. Buscaino, C. Wang, *et al.*, "Broadband electro-optic frequency comb generation in a lithium niobate microring resonator," Nature **568**, 373–377 (2019).
12. Y. Tang, J. Qiu, W. Ding, *et al.*, "Lithium niobate micro-waveguides for efficient supercontinuum generation and frequency comb self-referencing," Photonics Res. **13**, 3332–3340 (2025).
13. T.-H. Wu, L. Ledezma, C. Fredrick, *et al.*, "Visible-to-ultraviolet frequency comb generation in lithium niobate nanophotonic waveguides," Nat. Photonics **18**, 218–223 (2024).
14. C.-S. Brès, A. D. Torre, D. Grassani, *et al.*, "Supercontinuum in integrated photonics: generation, applications, challenges, and perspectives," Nanophotonics **12**, 1199–1244 (2023).
15. A. Boes, B. Corcoran, L. Chang, *et al.*, "Lithium niobate photonics: unlocking the electromagnetic spectrum," Laser Photonics Rev. **14**, 2000262 (2020).
16. L. Qu, W. Wu, W. Cai, *et al.*, "Second harmonic generation in lithium niobate on insulator," Laser Photonics Rev. **19**, 2401928 (2025).
17. W. Li and J. Zhang, "The journey of lithium niobate: history and recent advancements," Chin. Opt. **48**, 345–356 (2023).
18. Z. Wang, C. Wang, and H. Yu, "Advances in nonlinear photonic devices based on lithium niobate waveguides," J. Phys. D: Appl. Phys. **56**, 083001 (2023).
19. F. Ayhan, M. Ludwig, T. Herr, *et al.*, "Fabrication of periodically poled lithium niobate waveguides for broadband nonlinear photonics," APL Photonics **10**, 016118 (2025).
20. S. Liu, Y. Zheng, and X. Chen, "Nonlinear frequency conversion in lithium niobate thin films," Acta Opt. Sin. **41**, 0823013 (2021).
21. A. Rao, K. Abdelsalam, T. Sjaardema, *et al.*, "Actively-monitored periodic-poling in thin-film lithium niobate photonic waveguides with ultrahigh nonlinear conversion efficiency of 4600%$W^{-1}cm^{-2}$," Opt. Express **27**, 25920–25930 (2019).
22. C. Wang, C. Langrock, A. Marandi, *et al.*, "Ultrahigh-efficiency wavelength conversion in nanophotonic periodically poled lithium niobate waveguides," Optica **5**, 1438–1441 (2018).
23. P. Chen, I. Briggs, C. Cui, *et al.*, "Adapted poling to break the nonlinear efficiency limit in nanophotonic lithium niobate waveguides," Nat. Nanotechnol. **19**, 44–50 (2024).
24. Y. Tang, T. Ding, C. Lu, *et al.*, "Broadband second-harmonic generation in an angle-cut lithium niobate-on-insulator waveguide by a temperature gradient," Opt. Lett. **48**, 1108–1111 (2023).
25. C. Lu, Y. Zhang, J. Qiu, *et al.*, "Highly tunable birefringent phase matched second-harmonic generation in an angle-cut lithium niobate-on-insulator ridge waveguide," Opt. Lett. **47**, 1081–1084 (2022).
26. C. Wang, H. Zhong, M. Ning, *et al.*, "Broadband second harmonic generation in a z-cut lithium niobate on insulator waveguide based on type-I modal phase matching," Photonics **10**, 80 (2023).
27. Y. Tang, T. Ding, Y. Zhang, *et al.*, "Octave-spanning second-harmonic generation in dispersion-engineered lithium niobate-on-insulator microwaveguide," Adv. Photonics Res. **5**, 2400051 (2024).
28. L. Ge, Y. Chen, H. Jiang, *et al.*, "Broadband quasi-phase matching in a MgO:PPLN thin film," Photonics Res. **6**, 954–958 (2018).
29. J. Wang, X. Xue, J. Qiu, *et al.*, "Chirped periodically poled lithium-niobate-on-insulator micro-waveguides for broadband second-harmonic generation," Opt. Lett. **49**, 5348–5351 (2024).
30. X. Wu, L. Zhang, Z. Hao, *et al.*, "Broadband second-harmonic generation in step-chirped periodically poled lithium niobate waveguides," Opt. Lett. **47**, 1574–1577 (2022).
31. T. Yuan, J. Wu, X. Wang, *et al.*, "Chip-scale nonlinear bandwidth enhancement via birefringent mode hybridization," Adv. Photonics **6**, 056012 (2024).
32. I. Biaggio, V. Coda, and G. Montemezzani, "Coupling-length phase matching for nonlinear optical frequency conversion in parallel waveguides," Phys. Rev. A **90**, 043816 (2014).
33. B. Liu, H. Yu, Z. Y. Li, *et al.*, "Phase-matched second-harmonic generation in coupled nonlinear optical waveguides," J. Opt. Soc. Am. B **36**, 2650–2658 (2019).
34. M. Jankowski, C. Langrock, B. Desiatov, *et al.*, "Ultrabroadband nonlinear optics in nanophotonic periodically poled lithium niobate waveguides," Optica **7**, 40–46 (2020).
35. C. Zhang, X. Tian, H. Liu, *et al.*, "Ultrabroadband second-harmonic generation based on a dispersion-engineered lithium niobate on insulator waveguide," J. Opt. Soc. Am. B **39**, 3304–3310 (2022).
36. B. Chen, M. Ren, R. J. Liu, *et al.*, "Simultaneous broadband generation of second and third harmonics from chirped nonlinear photonic crystals," Light Sci. Appl. **3**, e189 (2014).